

UKAEA-CCFE-CP(22)03

A.R. Field, B. Chapman, D.R. Hatch, C.M. Roach, S.
Saarelma, L. Frassinetti

Comparing pedestal structure in JET- ILW H-mode plasmas with a model for stiff ETG turbulent heat transport

This document is intended for publication in the open literature. It is made available on the understanding that it may not be further circulated and extracts or references may not be published prior to publication of the original when applicable, or without the consent of the UKAEA Publications Officer, Culham Science Centre, Building K1/O/83, Abingdon, Oxfordshire, OX14 3DB, UK.

Enquiries about copyright and reproduction should in the first instance be addressed to the UKAEA Publications Officer, Culham Science Centre, Building K1/O/83 Abingdon, Oxfordshire, OX14 3DB, UK. The United Kingdom Atomic Energy Authority is the copyright holder.

The contents of this document and all other UKAEA Preprints, Reports and Conference Papers are available to view online free at scientific-publications.ukaea.uk/

Comparing pedestal structure in JET-ILW H-mode plasmas with a model for stiff ETG turbulent heat transport

A.R. Field, B. Chapman, D.R. Hatch, C.M. Roach, S. Saarelma, L. Frassinetti

Article submitted to journal

Subject Areas:

Magnetic Confined Fusion, Tokamak
Energy Confinement, Pedestal
electron heat transport

Keywords:

Pedestal, H-mode, heat transport,
stiffness, turbulence, ETG

Author for correspondence:

Anthony R Field e-mail:
anthony.field@ukaea.uk

Comparing pedestal structure in JET-ILW H-mode plasmas with a model for stiff ETG turbulent heat transport

A R Field¹, B Chapman-Oplolopoiou¹,
J W Connor¹, L Frassinetti², D R Hatch³,
C M Roach¹, S Saarelma¹ and JET
contributors*

¹ United Kingdom Atomic Energy Authority, Culham
Centre for Fusion Energy, Culham Science Centre,
Abingdon, Oxon, OX14 3DB, UK

² Division of Fusion Plasma Physics, KTH, Stockholm,
Sweden

³ Institute for Fusion Studies, University of Texas at
Austin, Austin, TX 78712, United States of America

*see the author list of [1]

A predictive model for the electron temperature profile of the H-mode pedestal is described and its results compared with the pedestal structure of JET-ILW pulses. The model is based on a scaling for the gyro-Bohm normalised, turbulent electron heat flux $q_e/q_{e,gB}$ resulting from electron-temperature gradient (ETG) turbulence, derived from results of nonlinear gyrokinetic calculations for the steep gradient region. Using the local temperature gradient scale length L_{T_e} in the normalisation, the dependence of $q_e/q_{e,gB}$ on the normalised gradients R/L_{T_e} and R/L_{n_e} can be represented by a unified scaling with the parameter $\eta_e = L_{n_e}/L_{T_e}$, to which the linear stability of ETG turbulence is sensitive when the density gradient is sufficiently steep. For a prescribed density profile, the value of R/L_{T_e} determined from this scaling, required to maintain a constant electron heat flux q_e across the pedestal, is used to calculate the temperature profile. Reasonable agreement with measurements is found for different cases, the model providing an explanation of the relative widths and shifts of the T_e and n_e profiles, as well as highlighting the importance of the separatrix boundary conditions. Other cases showing disagreement indicate conditions where other branches of turbulence might dominate.

© The Authors. Published by the Royal Society under the terms of the Creative Commons Attribution License <http://creativecommons.org/licenses/by/4.0/>, which permits unrestricted use, provided the original author and source are credited.

1. Introduction

The enhanced energy confinement of tokamak H-mode plasmas [2] is believed to result from $E \times B$ shear flow suppression of ion-scale turbulence ($k_y \rho_i \sim \mathcal{O}(1)$, where k_y is the wave number perpendicular to the flux surfaces and to the magnetic field B and ρ_i is the ion Larmor radius) [3] within a localised edge transport barrier (ETB) referred to as the pedestal, which forms just inside the last-closed flux surface (LCFS). The radial electric field within the ETB is proportional to the ion pressure gradient $E_r \sim p_i'/(enB)$ (where $' = d/dr$ and r is the minor radius) [4] and p' is maintained by the residual, conducted heat flux q_{cond} across the pedestal remaining after accounting for radiation and energy losses due to edge-localised modes (ELMs)¹ [5].

The predictive EPED model [6] for the total pressure at the pedestal top p_{ped} assumes that the pressure pedestal width Δ_p is determined by the stability of kinetic ballooning modes, which limit p' , yielding the relation $\Delta_p \propto \beta_p^{1/2}$, where β_p is the pedestal pressure normalised to the energy density of the poloidal magnetic field². The pedestal height is determined by increasing p_{ped} until the MHD stability limit set by peeling-ballooning instabilities [7] is reached, above which an ELM would be triggered. In order to determine the electron temperature at the pedestal top $T_{e,ped}$, which is required as a boundary condition for modelling the core temperature profiles, it is hence necessary to assume a prescribed pedestal density $n_{e,ped}$.

Typically, equal electron and ion temperatures ($T_e = T_i$) and equal widths for the electron density, temperature and pressure pedestals ($\Delta_{n_e} = \Delta_{T_e} = \Delta_p$) are assumed, which limits the veracity of predictions made using EPED. To improve the model, it is desirable to be able to predict the T_e profile given a prescribed density profile, which would obviate the necessity to assume equal temperature and density pedestal widths. Here, we present such a predictive model for the T_e profile based on a model for 'stiff'³ turbulent electron heat transport due to electron-temperature gradient driven (ETG) turbulence [8], which due to its fine spatial scale is not significantly affected by equilibrium $E \times B$ shear.

It was noted in Ref. [5] that in JET-ILW (ITER-like-wall) pedestals, the parameter $\eta_e = L_{n_e}/L_{T_e}$, where the gradient scale length is defined as $L_x = x/x'$, averaged across the steep density gradient region of the pedestal, appears to saturate at values $\langle \eta_e \rangle_{ped} \sim \mathcal{O}(2)$ at high heating power. Such observations have been made on various other tokamaks (see Refs. [75-81] of Ref. [11]). This value lies just above the linear stability threshold of ETG micro-instabilities of $\eta_e \sim 0.8$ [9], which is an indication that stiffness of the turbulent electron heat transport due to ETG turbulence may be limiting the T_e gradient across the pedestal.

A similar predictive pedestal model for the pedestal T_e profile to that presented here is discussed in Ref. [11], which is based on a scaling for the turbulent electron heat diffusivity χ_e derived from non-linear gyrokinetic calculations using the gyrokinetic code CGYRO [10] for the steep density gradient region of several different DIII-D pedestals. The scaling χ_e with η_e and the normalised temperature gradient R/L_{T_e} (where R is the major radius) proposed in Ref. [11] is shown to be consistent with that derived in similar study of JET-ILW pedestals presented in Ref. [12], upon which the model presented here is based. This suggests that a common mechanism underlies the turbulent electron heat transport across the pedestals studied in both devices.

Note that these models, which are both based on a critical η_e , appropriate for the steep-density gradient region, are not the only predictive models for the pedestal T_e profile. Heuristic models exist which are based on assumptions consistent with observations. An example of such a model [5], which assumes a constant η_e across the pedestal and infinite stiffness, i.e. η_e clamped at $\eta_{e,cr}$, is discussed in §5. An alternative model is that of Luda [14], which is based on observations that the parameter $T_{e,ped}/\langle T_e' \rangle_{ped} \sim 2$ cm (where $\langle T_e' \rangle_{ped}$ is the average pedestal T_e gradient) has been found to be relatively constant for a subset of pedestals on several devices [15]. This is

¹ELMs are explosive, edge-localised instabilities, which occur when the pedestal pressure reaches the MHD stability limit.

²The normalised poloidal pressure is defined as: $\beta_p = 2p_e/(2\mu_0 \bar{B}_p^2)$, where \bar{B}_p is the flux-surface averaged poloidal magnetic field.

³Turbulent transport is considered stiff when the associated heat flux increases more strongly than linearly with the driving temperature gradient above that required to kindle the turbulence.

then used in a transport model, together with an assumed pedestal width, to determine the heat diffusivity χ_e across the pedestal that satisfies this condition.

The justification for this model discussed in Ref. [14] is that this normalised temperature gradient R/L_{T_e} averaged over the pedestal, ‘*might be interpreted as the drive for turbulent transport, and therefore can be associated with electron temperature gradient (ETG) modes or micro-tearing modes (MTM)*’. However, from the discussion above and Refs [11,12], we learn that in the steep-density gradient region, ETG turbulence exhibits a threshold $\eta_{e,cr}$ rather than a threshold $R/L_{T_e,cr}$. Also, as can be seen in the JET-ILW pedestal profiles shown in the figures below, R/L_{T_e} varies considerably across the pedestal, so the electron heat transport is not governed by a constant critical value of this parameter.

The threshold behaviour of ETG turbulence is dependent on the magnitude of the normalised density gradient R/L_{n_e} . In the steep-density gradient region of the pedestal, where $R/L_{n_e} \sim \mathcal{O}(10 - 100)$, the critical temperature gradient $R/L_{T_e,cr} \propto R/L_{n_e}$, hence there is a critical $\eta_{e,cr}$ for finite growth rate. However, as discussed in Ref. [9], when the density gradient is weak, e.g. inside the top of the pedestal where $R/L_{n_e} \sim \mathcal{O}(1 - 10)$, $R/L_{T_e,cr}$ is expected to be independent of R/L_{n_e} and to be a function of other parameters, e.g. $R/L_{T_e,cr}(\hat{s}/q, \tau, \kappa, \epsilon, \dots)$, where the magnetic shear $\hat{s} = r q' / q$, $\tau = Z_{eff} T_e / T_i$, κ is the elongation and the inverse aspect ratio $\epsilon = r / R$.

These different threshold behaviours of ETG turbulence reflect the different dynamics in the presence of a strong or weak density gradient. The first case with the critical $\eta_{e,cr}$ corresponds to the ‘slab’ branch when the parallel resonance ($\omega \sim v_{th,e} k_{\parallel}$, where $v_{th,e}$ is the electron thermal velocity and k_{\parallel} is the parallel wave number) dominates the dynamics, while the second corresponds to the ‘toroidal’ branch when cross-field (curvature and grad-B) drifts dominate [13]. In the GENE simulations for the steep-density gradient region of JET-ILW pedestals discussed in Ref. [12], an increasing contribution of high- k_{\parallel} slab modes to the heat flux is observed when R/L_{T_e} is large and the ETG turbulence is driven hard.

Other studies have shown ETG modes to be dominant in the steep gradient region of JET-ILW pedestals, e.g. in Ref. [16], it is shown that ETG turbulence conducts $\sim 80\%$ of the conducted power in the electron channel. In Ref. [17], it is shown that for a particular JET-ILW equilibrium, similar to that of the 1.4 MA pulses discussed in §4(a) below, the dominant modes are a novel type of toroidal ETG mode, driven far from the mid-plane, with a large spatial scale ($k_y \rho_i \sim \mathcal{O}(1)$).

The remainder of this paper is structured as follows: In §2 the underlying physics of the model presented here is explained, which is based on a scaling of the locally gyro-Bohm normalised, turbulent electron heat flux with η_e , calculated using the actual, local L_{T_e} in the pedestal. This scaling can then be used for numerical integration of the pedestal T_e profile for a prescribed n_e profile, as described in §3. In §4, this method is used to calculate the pedestal T_e profile and compares the results with measured pedestal profiles for several different JET-ILW pulses. A simple analytic model of the pedestal T_e profile based on a constant $\eta_{e,cr}$ is discussed in §5, as is an interesting case when the numerical model fails, for which an alternative heat-flux scaling is proposed. Finally, the conclusions of this study and outlook for further work are presented in §6.

2. The ETG heat flux manifold

Recent non-linear, gyrokinetic simulations for JET-ILW H-mode plasmas using the gyrokinetic code GENE [18] have been used to quantify the stiffness of the saturated, turbulent electron heat flux q_e in the steep density gradient region of the pedestal [12].

A set of simulations were run in which the normalised gradients of temperature R/L_{T_e} and density R/L_{n_e} were scanned independently around the nominal experimental value, holding the corresponding parameter fixed. The resulting electron heat flux q_e normalised to a constant gyro-Bohm heat flux $q_{e,gB}$ was found to scale as $q_e/q_{e,gB} \propto (R/L_{n_e})^{-1}$ for the R/L_{n_e} scan and $\propto (R/L_{T_e} - R/L_{T_e,cr})^3$ for the R/L_{T_e} scan. Here, $q_{e,gB}$ is calculated using the nominal experimental parameters and is defined using the major radius R as the gradient scale length:

$q_{e,gB} = n_e \chi_{e,gB} T_e / R$ where $\chi_{e,gB} = v_{th,e} \rho_e^2 / R$, $v_{th,e}$ is the electron thermal velocity and ρ_e is the electron Larmor radius. For slab-ETG modes, the critical normalised temperature gradient is proportional to that of the density, i.e. $R/L_{T_e,cr} = \eta_{e,cr} R/L_{n_e}$, where the linear stability threshold $\eta_{e,cr} \sim 0.8$ [9].

Similar non-linear simulations using the CGYRO gyrokinetic code [10] have been used to determine the scaling of the electron heat flux in the steep gradient region of DIII-D H-mode pedestals [11]. The resulting scaling of $\chi_e/\chi_{e,gB}$ with η_e is used in a numerical pedestal model to compute the T_e profile. By using the actual, local value of L_{T_e} in each simulation to calculate the gyro-Bohm normalisation rather than the fixed scale length R , the resulting scaling (for six different cases, at three radial locations in two different pulses) could be approximated by the linear relation:

$$\chi_e = \alpha(\eta_e - \eta_{e,cr})(v_{th,e} \rho_e^2 / L_{T_e}) \equiv \alpha(\eta_e - \eta_{e,cr}) \chi_{e,MgB} \quad (2.1)$$

with the fitted constant $\alpha \sim 1.5$ and non-linear threshold $\eta_{e,cr} \sim 1.4$. Here, we have introduced the modified gyro-Bohm diffusivity defined using the local L_{T_e} as $\chi_{e,MgB} = \chi_{e,gB} (R/L_{T_e})$. Similarly, the local gyro-Bohm heat flux defined using the local L_{T_e} is referred to here as $q_{e,MgB} = q_{e,gB} (R/L_{T_e})^2$, as in Ref. [12].

Remarkably, in Ref. [12] it is shown that the results of these two separate studies can be represented by the same, approximate linear scaling in η_e , with nearly the same fit coefficients α and $\eta_{e,cr}$. In the JET-ILW study, gradients scans were performed for the same two 1.4 MA H-mode pulses with 16 MW of heating power with ‘low’ and ‘high’ rates of gas fuelling for which pedestal profiles are shown in Fig. 2 below.

In the following, $Q_e^* = q_e/q_{e,MgB}$ denotes the electron heat flux normalised to the modified gyro-Bohm heat flux. Fits of the turbulent heat flux data from these GENE scans to a linear scaling for Q_e^* of the form:

$$Q_e^* \equiv q_e/q_{e,MgB} \equiv \chi_e/\chi_{e,MgB} = \alpha(\eta_e - \eta_{e,cr}) \quad (2.2)$$

which follows from Eq. (2.1), gave values of $\alpha = 1.19$ and $\eta_{e,cr} = 1.49$ for the scans at low fuelling rate and $\alpha = 1.7$ and $\eta_{e,cr} = 1.9$ for the scans at high fuelling rate, while a fit to both data sets together yielded $\alpha = 1.74$ and $\eta_{e,cr} = 1.81$.

Note that a non-linear fit of the form:

$$Q_e^* = \alpha(\eta_e - \eta_{e,cr})^\beta \quad (2.3)$$

was found to better represent the data from both data sets with $\alpha = 0.85$, $\beta \sim 1.43$ and $\eta_{e,cr} = 1.28$, i.e. with a somewhat stronger than linear dependence on $\eta_e - \eta_{e,cr}$. In the analytic model presented below, the linear form in η_e is used as this is algebraically tractable. The results from this analytic model can then be used to provide an initial estimate of R/L_{T_e} as input to an iterative, numerical algorithm used to solve the non-linear scaling Eq. (2.3) for R/L_{T_e} .

It is straightforward to show how the q_e dependencies for the scans of R/L_{n_e} and R/L_{T_e} found in Ref. [12] and discussed above are consistent with Eq. (2.1), at least in the limit that $\eta_e \gg \eta_{e,cr}$. Eq. (2.2) can be expressed in terms of R/L_{T_e} and R/L_{n_e} as:

$$q_e/q_{e,gB} = \alpha(R/L_{n_e})^{-1}(R/L_{T_e} - R/L_{T_e,cr})(R/L_{T_e})^2 \quad (2.4)$$

where the non-linear threshold $R/L_{T_e,cr} = \eta_{e,cr}(R/L_{n_e})$. This relation encapsulates both the inverse dependence of $q_e/q_{e,gB}$ on R/L_{n_e} and, in the limit that $R/L_{T_e} \gg R/L_{T_e,cr}$, its cubic dependence on R/L_{T_e} . It is a theoretical prediction that, far above threshold, the turbulent heat flux of critically-balanced, saturated turbulence should scale as $q_e/q_{e,gB} \propto (R/L_{T_e})^3$ [19].

A relation such as Eq. (2.4) can be referred to as a heat flux ‘manifold’, i.e. in this case the surface $Q_e^*(R/L_{n_e}, R/L_{n_e})$. Such a manifold is shown in Fig. 1, in this case described by the relation:

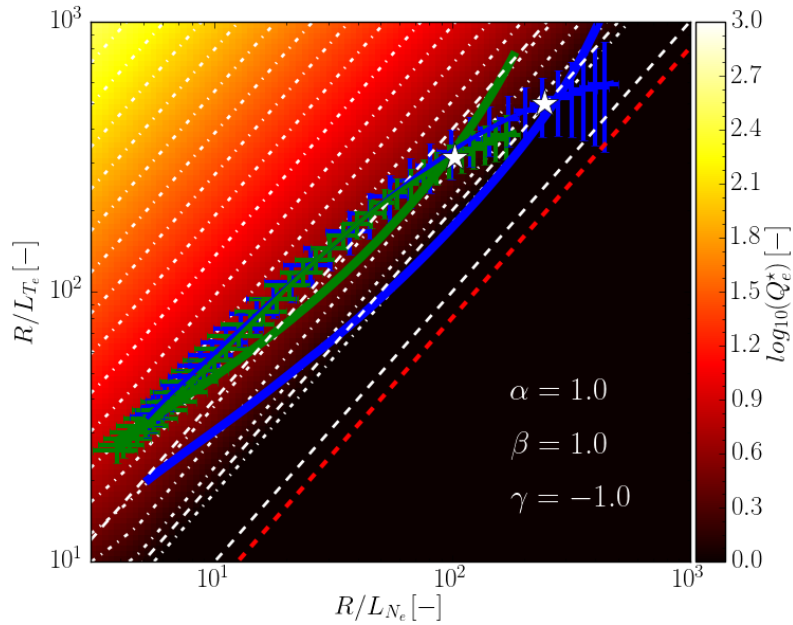


Figure 1. The normalised electron heat flux manifold $Q_e^*(R/L_{n_e}, R/L_{T_e})$ described by Eq. (2.5) assuming $\alpha = \beta = 1$ and $\gamma = -1$. The diagonal (white-dashed) lines correspond to $\eta_e = 1, 2, 4$ (bottom-top) and the contours (white-dotted) are at constant Q_e^* . The linear ETG stability threshold $R/L_{T_e,cr} = 0.8R/L_{n_e}$ from [9] is also shown (red-dashed). The lines with uncertainties show experimental loci $(R/L_{n_e}, R/L_{T_e})$ of the two sets of pedestal profiles shown in Fig. 2 for JET-ILW 1.4 MA H-mode pulses at 16 MW of heating with low (blue) and high (green) rates of gas fuelling together with the corresponding predictions of the stiff ETG model (solid lines). Note that the white stars indicate the mid-pedestal location for which the GENE simulations were performed.

$$Q_e^* = \alpha(R/L_{T_e} - R/L_{T_e,cr})^\beta (R/L_{n_e})^\gamma \quad (2.5)$$

With the parameters $\beta = 1$ and $\gamma = -1$ and $R/L_{T_e,cr} = \eta_{e,cr} R/L_{n_e}$, this form is equivalent to Eq. (2.4). In Fig. 1, the linear threshold $R/L_{T_e,cr}$ for ETG turbulence from Ref. [9] is used which is equivalent to assuming $\eta_{e,cr} = 0.8$ at sufficiently high values of R/L_{n_e} that the slab branch of ETG turbulence is prevalent, as is appropriate for the density steep-gradient region of the pedestal. Note that on this manifold, contours of constant η_e , which are diagonal lines in $(\log(R/L_{n_e}), \log(R/L_{T_e}))$ space, are also lines of constant Q_e^* . Note that these are not necessarily contours of the absolute heat flux q_e because $Q_e^* \propto q_e / (n_e T_e^{1/2} T_e'^2)$.

The heat flux manifold shown in Fig. 1 is shown overlaid by the experimental loci, i.e. the trajectory formed by pairs of values $(R/L_{n_e}, R/L_{T_e})$ across the pedestal, determined from the pre-ELM pedestal profiles for two 1.4 MA/1.7 T JET-ILW D pulses (#84794 & #87342) with similar heating powers of 16 & 14 MW respectively but with low and high rates of gas fuelling, i.e. $\Gamma_{D2} = 0.3$ and 1.8×10^{22} e/s, from which it can be seen that these loci *approximately* follow contours of constant $\eta_e \sim 2 - 4$.

This behaviour can be understood as follows. As the turbulent heat transport is stiff, i.e. approximately $q_e \propto (R/L_{T_e} - R/L_{T_e,cr})^3$, we may expect the temperature gradient T_e' to adjust such that the absolute electron heat flux q_e remains constant across the pedestal (as would be expected with minimal sources and sinks in the pedestal), with the resulting profiles ensuring that the locally gyro-Bohm normalised heat flux Q_e^* follows approximately contours of constant η_e not far above the threshold $\eta_{e,cr}$ for the onset of turbulence. In other words, when $\eta_e - \eta_{e,cr} > \mathcal{O}(1)$,

i.e. at values of $\eta_e \sim \mathcal{O}(2)$ where $Q_e^* \sim \mathcal{O}(1)$, the absolute heat flux increases rapidly with R/L_{T_e} , hence clamping the experimental $(R/L_{n_e}, R/L_{n_e})$ loci to contours of approximately constant $\eta_e \sim \mathcal{O}(2)$. It is shown in §3 below how this property, embodied in Eq. (2.4) can be used to predict the temperature profile for a prescribed density profile and boundary conditions at the separatrix.

3. Numerical model for T_e profile

At each flux surface across the pedestal of area S , the electron temperature gradient T_e' will adjust such that the ETG turbulence conducts the imposed heat flux from the plasma interior, i.e. $q_e = P_{e,cond}/S$, where $P_{e,cond}$ is the conducted electron loss power. For simplicity, energy losses from the electrons due to ionisation, radiation and collisional exchange with the ions are neglected.⁴ Hence, $P_{e,cond}$ is assumed to be the same as the electron loss power $P_{e,sep}$ crossing the LCFS. Furthermore, the relatively small fractional change in the flux surface area across the narrow pedestal region is neglected, i.e. $q_e = P_{e,sep}/S_{sep}$, where S_{sep} is the area of the LCFS.⁵

If we assume that the turbulent electron heat flux obeys the scaling given by Eq. (2.4), in order to calculate the T_e profile by numerical integration, it is necessary to solve this cubic equation in R/L_{T_e} at each flux surface. Note that we expect this relation to be appropriate for the steep-gradient region of the pedestal, for which the non-linear gyrokinetic calculations were performed but we might expect departures from this scaling, e.g. inside the density pedestal top, where the density gradient is weaker and the electron scale turbulence has different characteristics.

The scaling given by Eq. (2.4) can be expressed as:

$$(R/L_{n_e})^{-1}(R/L_{T_e})^3 - \eta_{e,cr}(R/L_{T_e})^2 - q_e/(\alpha q_{e,gB}) = 0 \quad (3.1)$$

i.e. as a cubic polynomial $ax^3 + bx^2 + cx + d = 0$ in $x = R/L_{T_e}$, where $a = (R/L_{n_e})^{-1}$, $b = -\eta_{e,cr}$, $c = 0$ and $d = -q_e/(\alpha q_{e,gB})$. As all of these quantities are positive definite, it is simple to determine whether the discriminant⁶ of the polynomial $\Delta < 0$, thus proving there is only one real root, which is the case for the calculations presented here.

In order to calculate $q_{e,gB} = en_e T_e v_{th,e} (\rho_e/R)^2$, with $v_{th,e} = (2eT_e/m_e)^{1/2}$, $\rho_e = v_{th,e}/\Omega_e$ and the electron gyro frequency $\Omega_e = eB/m_e$, the parameters T_e , n_e and B are required. For the coefficients of Eq. (3.1), the parameter R/L_{n_e} from the prescribed n_e profile, the electron heat flux q_e and the coefficients of the ETG heat flux scaling α and $\eta_{e,cr}$ are required.

Numerical integration of the T_e profile requires starting at the separatrix with prescribed values of $T_{e,sep}$ and $n_{e,sep}$, e.g. as determined from measurements or from a SOL plasma model, assuming a prescribed density profile from which the profile of R/L_{n_e} is calculated, and a particular value of $q_e = P_{e,sep}/S_{sep}$ and then using these to solve Eq. (3.1) for R/L_{T_e} .

The value of R/L_{T_e} at the particular flux surface is then used in an explicit, forward integration to calculate the temperature at the next integration step $T_e[i+1]$, starting at the separatrix, where $T_e[0] = T_{e,sep}$ by iteration of:

$$T_e[i+1] = T_e[i](1 + (R/L_{T_e})) [i](\delta R/R[i]) \quad (3.2)$$

where $[i]$ is the i^{th} radial element of a vector and δR is the radial integration increment. A fixed value of T_e at the separatrix is often assumed for JET-ILW H-mode plasmas of $T_{e,sep} \sim 100$ eV. This is justified because $T_{e,sep}$ is a weak function of the loss power $P_{e,sep}$ [26].

Numerical solution of the non-linear form of the heat flux scaling given by Eq. (2.3), i.e. $Q_e^* = \alpha (\eta_e - \eta_{e,cr})^\beta$, has been implemented. This algorithm uses the analytic solution of Eq. (2.4) to provide an initial guess for R/L_{T_e} (and hence η_e), which is then repeatedly incremented by

⁴Note that charge-exchange reactions with cold neutral atoms is an energy loss from the ion channel, not the electrons. Also, as discussed in §5, power losses due to ionisation and radiation directly from the pedestal region are relatively small compared to that conducted through the pedestal through the electron channel $P_{e,cond}$.

⁵The effect of neglecting the fractional change in the flux surface area ($S \propto \psi_N$, where ψ_N is the normalised poloidal flux enclosed by the surface) across the pedestal is small compared to other approximations made in the analysis, i.e. $\Delta S \sim 5\%$ across the typical width of the pedestal $\Delta n_e \sim 0.05$ expressed in terms of ψ_N .

⁶The discriminant of a cubic polynomial is defined in terms of its coefficients as $\Delta = \frac{4(b^2 - 3ac)^3 - (2b^3 - 9abc + 27a^2d)^2}{27a^2}$.

a small fraction until the non-linear scaling is satisfied. Unless otherwise stated, the model T_e profiles presented in the figures here are calculated assuming this non-linear form, using the nominal coefficients $\alpha = 0.85$, $\beta = 1.28$ and $\beta = 1.43$, as appropriate for the 1.4 MA, low and high-gas JET-ILW pulses discussed in §4(a).

4. Comparison of predicted with measured pedestal T_e profiles

As a first test of the model described in §3 above, predicted T_e profiles for JET-ILW H-mode pulses with different rates of gas fuelling, plasma currents and heating powers are compared with the experimentally measured profiles. Note that, whereas the 1.4 MA, low-triangularity (δ) pulses are the same as those used in Ref. [12] to determine the turbulent heat flux scaling, also including higher current 3.5 MA pulse at high heating power with quite different parameters allows a more stringent test of the predictive capability of the model. The parameters of the analysed pulses are given in Table 1. Note that the loss power components during the inter-ELM periods due to radiation P_{Rad}^{iELM} , ELMs $\langle P_{ELM} \rangle$ and inter-ELM heat transport P_{sep}^{iELM} are determined using the method described in Ref. [5].

Pulse #	I_p [MA]	B_t [T]	P_{in} [MW]	Γ_{D2} [10^{22} e/s]	$t_0 - t_1$ [s]	P_{Rad}^{iELM} [MW]	$\langle P_{ELM} \rangle$ [MW]	P_{sep}^{iELM} [MW]
84794	1.4	1.7	16.0±0.3	0.3	5.0-6.0	3.8±0.2	3.4±0.2	6.2±0.7
87342	1.4	1.7	13.9±0.4	1.8	5.5-8.8	1.3±0.2	7.2±0.1	5.4±0.5
96482	3.5	3.3	32.1±0.1	2.1	9.5-10.5	16.0±0.1	5.3±0.2	10.9±0.3
94662	3.0	2.8	26.1±0.1	0.0	9.0-10.0	11.3±0.1	5.5±0.2	9.3±0.3

Table 1. Parameters of the JET-ILW pulses discussed in §4: plasma current I_p , toroidal field B_t , input power P_{in} , D_2 gas fuelling rate Γ_{D2} , averaging period $t_0 - t_1$ and the loss power components due to radiation, ELMs (time averaged) and inter-ELM heat transport. Note that pulse #96482 was fuelled by both gas puffing and cryogenic deuterium ELM pacing pellets, injected at a repetition rate of ~ 35 Hz.

For the 1.4 MA high-gas pulse #87342 with ~ 14 MW heating power, a high ELM frequency ($f_{ELM} \sim \mathcal{O}(100)$ Hz) prevented determination of $\langle P_{ELM} \rangle$ from changes in the plasma stored energy W_{pl} determined from magnetic measurements as described in Ref. [5], so the same fraction of ELM loss power to the total heating power of $\langle P_{ELM} \rangle / P_{in} \sim 0.52$ is assumed as in the lower power ~ 5 MW pulse #87346 at the same fuelling rate for which f_{ELM} was low enough to determine $\langle P_{ELM} \rangle$ reliably⁷

(a) 1.4 MA/1.7 T low- δ pulses at low & high-fuelling rates

Pedestal profiles for two 1.4 MA, low- δ H-mode pulses with low and high rates of D_2 gas fuelling (#84794 and #87342 at $\Gamma_{D2} \sim 0.3$ & 1.8×10^{22} e/s, with 16 & 14 MW of heating power respectively) [20,21] are shown in Fig. 2. The T_e and n_e profiles are $\text{mtanh}()$ fits [22,23] to an ensemble of measured profiles from the high-resolution Thompson scattering system (HRTS) [24] from the pre-ELM phase of several inter-ELM periods, which are taken from the EUROfusion pedestal database [25]. Both profiles are shifted radially to ensure that $T_{e,sep} \sim 100$ eV, which is a typical value for JET-ILW [26] and mapped onto the normalised poloidal flux coordinate ψ_N using a magnetic equilibrium reconstructions from EFIT [27].

Global linear GENE simulations presented in Ref. [12] for these cases (in which $T_i = T_e$ was assumed), show that ion scale modes that would be responsible for any ion scale turbulent heat flux are largely suppressed by $E \times B$ flow shear and also that collisional, neo-classical ion heat

⁷Note that it was found in Ref. [5] that for the low-gas 1.4 MA pulses these loss power fractions were quite constant across the heating power scan.

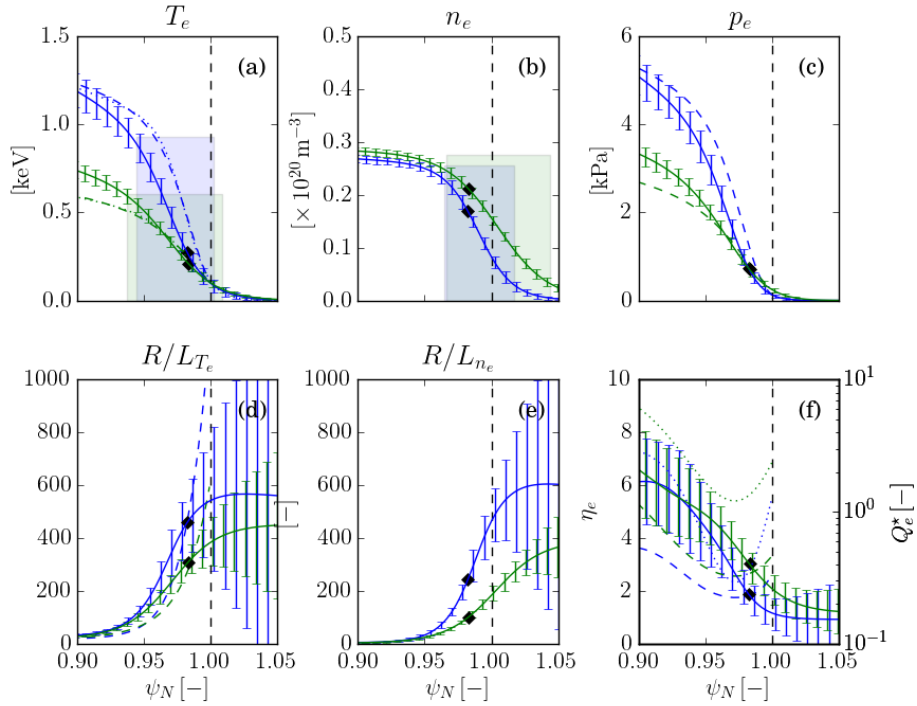


Figure 2. Pre-ELM averaged ($\sim 80 - 100\%$ of the inter-ELM period) pedestal profiles for two 1.4 MA JET-ILW H-mode pulses at low (#84794, blue) and high (#87342, green) rates of D gas fuelling with 16 & 14 MW of heating power respectively showing (with error bars): (a) electron temperature T_e , (b) density n_e , (c) pressure p_e , their normalised gradients (d) R/L_{T_e} , (e) R/L_{n_e} and (e) the parameter η_e (solid/dashed) and the locally gyro-Bohm normalised electron heat flux Q_e^* (dotted) vs' normalised poloidal flux ψ_N . The height, width and position of the $\text{mtanh}()$ fits to the measured T_e and n_e profiles are indicated by the shaded bars. Profiles in (a, c, d and f) calculated using the stiff ETG model assuming the scaling: $Q_e^* = 0.85(\eta_e - 1.28)^{1.43}$ are shown dashed with $\text{mtanh}()$ fits to the calculated profiles (dotted). The mid-pedestal locations at which the GENE calculations were performed are indicated by the \blacklozenge symbols. The uncertainties on the fitted profiles are obtained using a Monte-Carlo method using the uncertainty estimates on the fit parameters.

transport accounts for $\lesssim 20\%$ of the inter-ELM heat transport ($P_{i,NC} \sim 1.2$ MW in #84794 and ~ 0.6 MW in #87342). For calculation of the predicted T_e profiles, it is assumed that the residual, conducted power across the pedestal during the inter-ELM periods is carried by turbulent electron heat transport, i.e. $P_{e,sep} = P_{sep}^{iELM} - P_{i,NC}$.

The effect of increasing the fuelling rate Γ_{D2} between the two pulses shown in Fig. 2 by a factor ~ 6 is to increase the separatrix density $n_{e,sep}$, while the pedestal density $n_{e,ped}$ remains largely unchanged, i.e. the relative separatrix density $n_{e,sep}/n_{e,ped}$ is approximately doubled. This increase reduces the normalised density gradient R/L_{n_e} across the steep gradient region of the pedestal. Note that for both pulses the profile of η_e increases from values $\sim 2 - 3$ in the steep density gradient to ~ 6 at the top of the T_e pedestal, i.e. there is a concomitant decrease of R/L_{T_e} across the pedestal which partially compensates the decrease of R/L_{n_e} to maintain similar profiles of η_e . The result of reducing R/L_{T_e} across the pedestal at a constant separatrix temperature $T_{e,sep}$ is to progressively decrease T_e inwards across the pedestal, almost halving the pedestal top temperature $T_{e,ped}$.

Pulse #	$n_{e,ped}$ [$10^{20}m^{-3}$]	$n_{e,sep}/n_{e,ped}$ [-]	$T_{e,ped}$ [keV]	Δn_e [ψ_N]	$\Delta T_e/\Delta n_e$ [ψ_N]	δ_{n-T} [ψ_N]
84794	0.26±0.01	0.33±0.05	0.93±0.05	0.05±0.01	0.57±0.06	0.017 ± 0.003
87342	0.28±0.01	0.57±0.03	0.61±0.03	0.08±0.01	0.36±0.03	0.032 ± 0.003
96482	0.51±0.01	0.53±0.02	0.86±0.02	0.032±0.003	0.91±0.13	0.012 ± 0.001
94662	0.28±0.01	0.37±0.04	1.02±0.07	0.065±0.01	0.81±0.13	0.018 ± 0.004

Table 2. Pedestal parameters of the JET-ILW pulses discussed in §4: n_e and T_e at pedestal top, pedestal widths $\Delta n_e, \Delta T_e$ in ψ_N , relative shift δ_{n-T} of density and temperature pedestal positions and relative separatrix density.

Although the pedestal profiles look rather different for the two cases, the corresponding loci ($R/L_{n_e}, R/L_{T_e}$) shown in Fig. 1 almost overlay but importantly, the low-gas case (#84794) extends to higher values of R/L_{n_e} and R/L_{T_e} towards the separatrix. In the high-gas case, the effect of increasing $n_{e,sep}$ (and hence decreasing R/L_{n_e} across the pedestal) is to reduce the values of R/L_{T_e} required to maintain the normalised heat flux Q_e^* corresponding to a constant absolute turbulent heat flux q_e across the pedestal. At a given η_e , decreasing n_e at the separatrix necessitates starting the integration of the T_e profile with a higher gradient $T_e' = \eta_e T_{e,sep}(n_e'/n_{e,sep})$, this effect propagating inwards, increasing T_e across the whole pedestal.

Pedestal parameters determined from the fitted profiles for the various cases are stated in Table 2 and compared with similar parameters for the T_e profiles calculated using the stiff ETG model in Table 3. For the low-gas pulse #84794, $T_{e,ped}$ is close to the measured value ($\times 0.97$), while the T_e pedestal width ΔT_e is under predicted ($\times 0.65$). This is because the values of R/L_{T_e} required to satisfy the Q_e^* scaling are too large outside the mid-pedestal location at which the GENE calculations were performed, hence increasing T_e across the steep-gradient region. However, this is compensated by too low a value of R/L_{T_e} inside the mid-pedestal location, resulting overall in a reasonable prediction of $T_{e,ped}$ but a reduced pedestal width ΔT_e .

For the high-gas pulse #87342, $T_{e,ped}$ is somewhat under predicted ($\times 0.76$), while the predicted ΔT_e is closer to the measured value ($\times 0.8$) than for the low-gas pulse. Note that the observation that the actual temperature pedestal is considerably narrower than the density pedestal, i.e. $\Delta T_e/\Delta n_e \sim 0.57$ and ~ 0.36 in both the low- and high-gas cases respectively, is reproduced by the model.

Note that in the high gas pulse #87342, the locally gyro-Bohm normalised electron heat flux Q_e^* is a factor $\sim 2 - 4$ larger than in the low-gas pulse #84794 (see Fig. 2 (f)), as a consequence of the weaker T_e gradient in the former driving a similar absolute electron heat flux. Note that in the steep-gradient region of the pedestal $Q_e^* \lesssim \mathcal{O}(1)$, while at the pedestal top where R/L_{T_e} is much weaker, Q_e^* is up to an order of magnitude larger. It is discussed in Ref. [11] that this difference might be explicable in terms of increasing anisotropy ($k_r/k_y < 1$) of the ETG turbulence as this transitions from the slab to the toroidal branch at higher values of η_e .

Pulse #	Case	$T_{e,ped}^{ETG}$ [keV]	ΔT_e^{ETG} [ψ_N]	$T_{e,ped}^{ETG}/T_{e,ped}$ [-]	$\Delta T_e^{ETG}/\Delta T_e$ [-]	α [-]	$\eta_{e,cr}$ [-]	β [-]	$T_{e,sep}$ [keV]
84794	A	0.90	0.037	0.97±0.05	0.65±0.12	0.85	1.28	1.43	0.1
87342	A	0.46	0.057	0.76±0.04	0.80±0.09	0.85	1.28	1.43	0.1
96482	A	0.51	0.023	0.59±0.02	0.79±0.08	0.85	1.28	1.43	0.1
96482	B	0.79	0.019	0.91±0.02	0.66±0.07	0.85	1.28	1.43	0.065
94662	A	1.37	0.034	1.33±0.1	0.65±0.07	0.85	1.28	1.43	0.1
94662	B	0.91	0.041	0.89±0.06	0.76±0.09	0.85	0.8	2.9	0.1

Table 3. Parameters from $\text{mtanh}()$ fits to the calculated T_e profiles from the ETG model for the JET-ILW pulses discussed in §4: $T_{e,ped}^{ETG}$ at pedestal top and pedestal width ΔT_e^{ETG} in ψ_N , ratio of calculated and measured heights and widths, for cases with different assumed values for $\eta_{e,cr}$, β and $T_{e,sep}$ used for the calculation.

(b) 3.5 MA/3.3 T high-power, ITER-baseline scenario pulse

A more stringent test of the model is to apply it to a case from a pulse with quite different parameters as those for which the ETG heat flux scaling was determined, e.g. as offered by the high-power, 3.5 MA ITER-baseline scenario H-mode pulse #96482 with ~ 34 MW of heating power [28,29]. The high fraction of power radiated by W impurities in this pulse $\mathcal{F}_{Rad} \sim 0.5$ results in a loss power due to inter-ELM heat transport $P_{sep}^{iELM} \sim 11$ MW after accounting for the ELM loss power of $\langle P_{ELM} \rangle \sim 5.3$ MW, which is again determined using the method described in Ref. [5].

As reported in Ref. [16], non-linear gyrokinetic calculations of the pedestal heat transport have been performed for a similar high-power, JET-ILW 3 MA ITER-baseline scenario pulse #92432, the behaviour of which is also discussed in detail in Ref. [5]. In this case, with the assumption of realistic dilution by Be impurities, $\sim 80\%$ of the conducted loss power across the pedestal could be explained by ETG turbulence. Hence, in our calculations for #96482, we assume that all of the inter-ELM pedestal heat transport is conducted through the electron channel, i.e. $P_{e,sep} = P_{sep}^{iELM}$.

Pedestal profiles for this high-power 3.5 MA pulse #96482 are shown in Fig. 3. This pulse has a somewhat higher net fuelling rate from gas puffing and pellets $\Gamma_{D2} \sim 2.1 \times 10^{22}$ e/s to that of the high-gas, 1.4 MA pulse #87342 ($\sim 1.8 \times 10^{22}$ e/s), however, the relative separatrix density $n_{e,sep}/n_{e,ped} \sim 0.4$ is not as high as in the latter pulse (~ 0.6). This and the factor ~ 2 higher loss

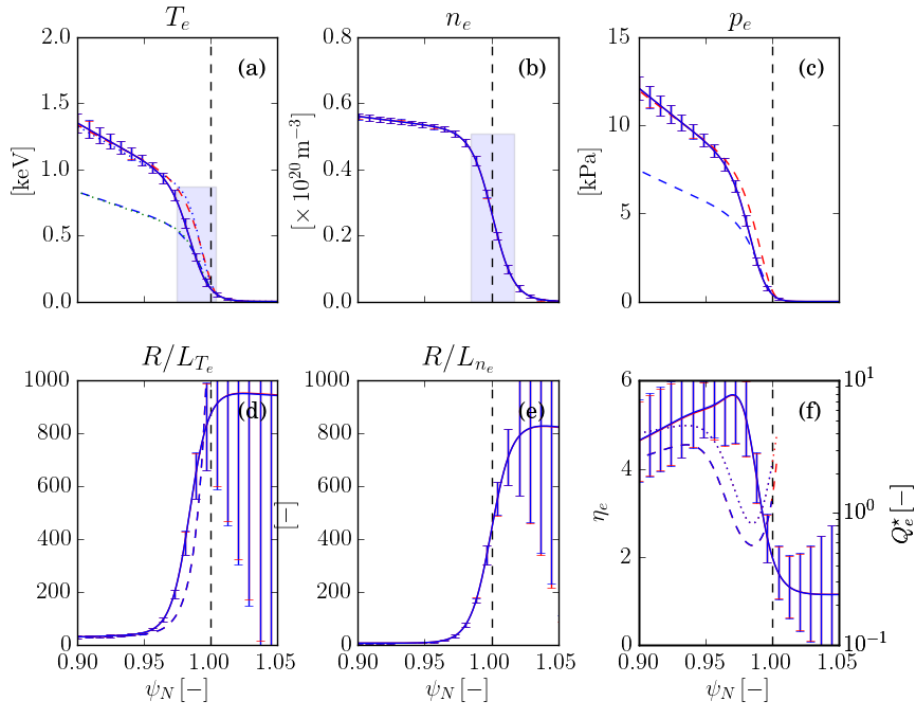


Figure 3. Pre-ELM averaged ($\sim 80 - 100\%$ of the inter-ELM period) pedestal profiles for the JET-ILW 3.5 MA/3.3 T ITER-baseline scenario pulse #96482 with 34 MW of heating power with deuterium gas fuelling and 35 Hz ELM-pacing pellets. Two cases with the parameters stated in Table 3 are shown using the nominal Q_e^* scaling parameters A (cyan) with $T_{e,sep} \sim 100$ eV and B (red) starting the integration where $T_e \sim 65$ eV.

power P_{sep}^{iELM} results in a $\sim \times 1.4$ higher $T_{e,ped} \sim 0.86$ keV than in the lower current, high gas pulse.

The most important difference between the pulses from the point of view of the predicted $T_{e,ped}$ is the value of toroidal field B , which is about twice as high in the 3.5 MA pulse than in the 1.4 MA pulses, i.e. 3.3 T c.f. 1.7 T. This reduces the gyro-Bohm normalisation $q_{e,gB} \propto 1/B^2$ in the heat flux scaling Eq. (2.4) by a factor $\times 0.26$, hence requiring a larger R/L_{Te} to match the prescribed heat flux q_e . In spite of this, the predicted $T_{e,ped} \sim 0.51$ keV is a factor ~ 0.6 below the actual value (case A in Table 3), while the width Δ_{Te} is better reproduced, namely to a factor ~ 0.8 of the actual value.

In §5, it is shown by means of an analytic model that a consequence of stiff ETG heat transport is a high sensitivity of the predicted $T_{e,ped}$ to the boundary conditions at the separatrix, in particular to the relative separatrix density $n_{e,sep}/n_{e,ped}$. Because of the steep gradient of R/L_{ne} at the separatrix, the predicted $T_{e,ped}$ is particularly sensitive to the separatrix location and uncertainties in the measured profiles. Reducing the assumed value of $T_{e,sep}$ from 100 eV to 65 eV decreases $n_{e,sep}$ ($\times 0.78$) and increases the initial value of R/L_{ne} ($\times 1.6$), consequently increasing the predicted $T_{e,ped}$, better matching the actual value ($\sim \times 0.93$) (case B in Table 3). Note that the two-point SOL model predicts that the separatrix temperature is a weak function of the loss power, i.e. $T_{e,sep} \propto P_{e,sep}^{2/7}$, so this is a rather large adjustment⁸.

Alternatively, the predicted $T_{e,ped}$ can also be increased by increasing the non-linear threshold $\eta_{e,cr}$ from the nominal value of 1.28, e.g. to 2.4, matching $T_{e,ped}$ to a factor $\times 0.91$. This purely conjectural change to the Q_e^* scaling could only be confirmed by means of further non-linear GK calculations. In all three cases, the normalised heat flux Q_e^* shown in Fig. 3 (f) is of similar magnitude and profile shape to that in the 1.4 MA pulses in Fig. 2.

5. Discussion

As discussed in §1, across the steep-density gradient region of the pedestal, the parameter η_e is typically observed to be $\sim \mathcal{O}(2)$. It is illuminating to consider the consequences for the predicted T_e profile of assuming: (i) that above a critical $\eta_{e,cr}$, the electron heat transport is infinitely stiff, i.e. clamping η_e at this threshold and (ii) that $\eta_{e,cr}$ is constant across the pedestal [5]. The definition of $\eta_e = L_{ne}/L_{Te}$ is actually a differential equation for T_e , i.e. $T_e' = \eta_e T_e (n_e'/n_e)$, which for constant $\eta_{e,cr}$ can be integrated analytically inwards from the separatrix to yield:

$$T_e(\psi_N) = T_{e,sep} \left(\frac{n_e(\psi_N)}{n_{e,sep}} \right)^{\eta_{e,cr}} \quad (5.1)$$

which highlights the importance of the boundary conditions at the separatrix in determining T_e across the pedestal if the heat transport is stiff. Referring to T_e at the top of the density pedestal as $T_{e,ped}^*$ Eq. (5.1) then gives: $T_{e,ped}^* \equiv T_e(\psi_N, n_{e,ped}) = T_{e,sep} (n_{e,ped}/n_{e,sep})^{\eta_{e,cr}}$.

This relation implies that, were very stiff heat transport to clamp η_e to the critical threshold, $T_{e,ped}$ would then be: (i) highly sensitive to the relative separatrix density $n_{e,sep}/n_{e,ped}$; (ii) independent of the electron heat flux q_e across the pedestal; and (iii) independent of the density pedestal width Δ_{ne} . Note that Ref. [30] discusses the role of the relative separatrix density in governing the turbulent heat transport across the pedestal in JET-ILW. Also, in Ref. [31] the effect of the relative shift δ_{n-T} on the MHD stability of the pedestal is investigated, showing that the reduced shift δ_{n-T} at low rates of gas puffing result in higher values of pedestal pressure $p_{e,ped}$.

Furthermore, it can be shown numerically that when $\eta_{e,cr} > 1$ across the pedestal, the predicted T_e profiles are shifted radially inwards with respect to the n_e profiles, i.e. $\delta_{n-T} = \psi_{N,n_{e,ped}} - \psi_{N,T_{e,ped}} > 0$, as is evident from the profiles shown in Fig. 2 and Fig. 3. Also, the predicted T_e pedestal width Δ_{Te} is narrower than that of the density Δ_{ne} and vice versa for $\eta_e < 1$. Of course, when $\eta_e = 1$ the shapes of the profiles are identical and $\delta_{n-T} = 0$. The actual

⁸The purpose of this speculative change to $T_{e,sep}$ is primarily to increase the value of R/L_{ne} at the separatrix, a quantity which has large measurement uncertainties due to its steep gradient.

Pulse #	$T_e(\psi_N^{n,top})$ [keV]	$\langle \eta_e \rangle_{ped}$ [-]	$T_{e,ped}^*$ [keV]	$T_{e,ped}^*/T_e(\psi_N^{n,top})$ [-]
84794	0.57 ± 0.06	1.9 ± 0.1	0.84 ± 0.3	1.5 ± 0.6
87342	0.36 ± 0.03	3.0 ± 0.1	0.54 ± 0.1	1.5 ± 0.3
96482	0.45 ± 0.03	3.1 ± 0.2	0.67 ± 0.14	1.5 ± 0.3
94662	0.79 ± 0.08	2.4 ± 0.4	1.1 ± 0.3	1.3 ± 0.4

Table 4. Parameters from the analytic model discussed in §5 for the JET-ILW pulses discussed in §4: T_e at density pedestal top, average value of η_e across the density pedestal, calculated value of $T_{e,ped}^*$ using Eq. (5.1) and the ratio of this estimate to the measured values.

values of Δ_{T_e} , Δ_{n_e} , their ratios and relative shifts δ_{n-T} listed in Table 2 qualitatively conform to this behaviour.

Average values of η_e across the density pedestal ($\psi_{N,n_{e,ped}} < \psi_N < 1$) stated in Table 4 are in the range $\langle \eta_e \rangle_{ped} \sim 2 - 3$. Using these values of $\langle \eta_e \rangle_{ped}$ and the measured values of $n_{e,ped}/n_{e,sep}$ stated in Table 4 in Eq. (5.1) yields values of $T_{e,ped}^*$, which are a factor ~ 1.5 higher than the actual values of $T_e(\psi_N^{n,top})$. Interestingly, it has been found for a heating power scan over the range 4.6 – 16 MA, including the same 1.4 MA low-gas pulses as discussed in §4(a), $\langle \eta_e \rangle_{ped}$ remains approximately constant across the steep-density region of the pedestal, while the increasing $T_{e,ped}$ with P_{in} can at least partly be attributed to $n_{e,sep}$ decreasing approximately as $P_{e,sep}^{-1/2}$, even when taking into account the weak dependence of $T_{e,sep}$ on the loss power $T_{e,sep} \propto P_{e,sep}^{2/7}$.

As shown in Fig. 4, when using the numerical model to predict the T_e profile for the atypical JET-ILW 3 MA pulse #94662 with 30 MW of heating and without gas puff fuelling during the sustained H-mode phase [32]⁹, using the nominal coefficients in the heat flux scaling determined for the 1.4 MA pulses, the resulting T_e is too high (by a factor of ~ 1.3) because of the high initial value of R/L_{T_e} obtained at the separatrix from the Q_e^* scaling.

For this ‘zero-gas’ pulse, the density pedestal is about twice as wide ($\Delta_{n_e} \sim 0.065$), while the relative separatrix density $n_{e,sep}/n_{e,ped} \sim 0.23$ is about half that as in the high-power 3.5 MA pulse #96482 shown in Fig. 3, which has a high rate of gas fuelling. The resulting low value of n_e at the separatrix then requires high values of R/L_{T_e} and η_e , which are much higher than the measured values, to conduct the prescribed electron heat flux q_e across this region, while η_e is actually approximately constant across the pedestal, with an average value $\langle \eta_e \rangle_{ped} \sim 2.4$.

By adopting a stiffer heat flux scaling of the form $Q_e^* \propto (\eta_e - 0.8)^{2.9}$, i.e. with $\eta_{e,cr}$ reduced from 1.28 to the linear ETG threshold and increasing the exponent, the T_e profile for this wide pedestal can be reproduced reasonably well, matching $T_{e,ped}$ to a factor $\times 0.89$ and Δ_{T_e} to a factor $\times 0.76$. Note that in this case, the alternative of shifting the profiles to higher $T_{e,ped}$ and hence decrease R/L_{n_e} at the separatrix is unable to reduce $T_{e,ped}$ sufficiently unless an unrealistically high value of ~ 500 eV is assumed.

The resulting profiles from the full ETG model of §3 confirm the observation for all cases considered here that R/L_{T_e} is overestimated outside the mid-pedestal and underestimated towards the pedestal top. This perhaps indicates that the actual electron heat transport is stiffer in the region just inside the separatrix but not as stiff towards the pedestal top as at the mid-pedestal location, particularly so for this low-collisionality pedestal.

It is unlikely that the heat losses from the electrons directly from the pedestal region due to ionisation and radiation are sufficient to significantly reduce q_e close to the separatrix. In Ref. [29], these power losses, estimated for the 3 MA JET-ILW baseline scenario pulse #92432 at 32 MW heating power with a similarly high gas fuelling rate to that in pulse #96482 are shown to be relatively small ($\lesssim \mathcal{O}(0.1$ MW) and $\lesssim \mathcal{O}(1$ MW) due to ionisation and radiation respectively) compared to the power conducted across the pedestal through the electron channel O (10 MW). In

⁹Note that there is fuelling from neutral deuterium recycling in the divertor but no direct gas puffing.

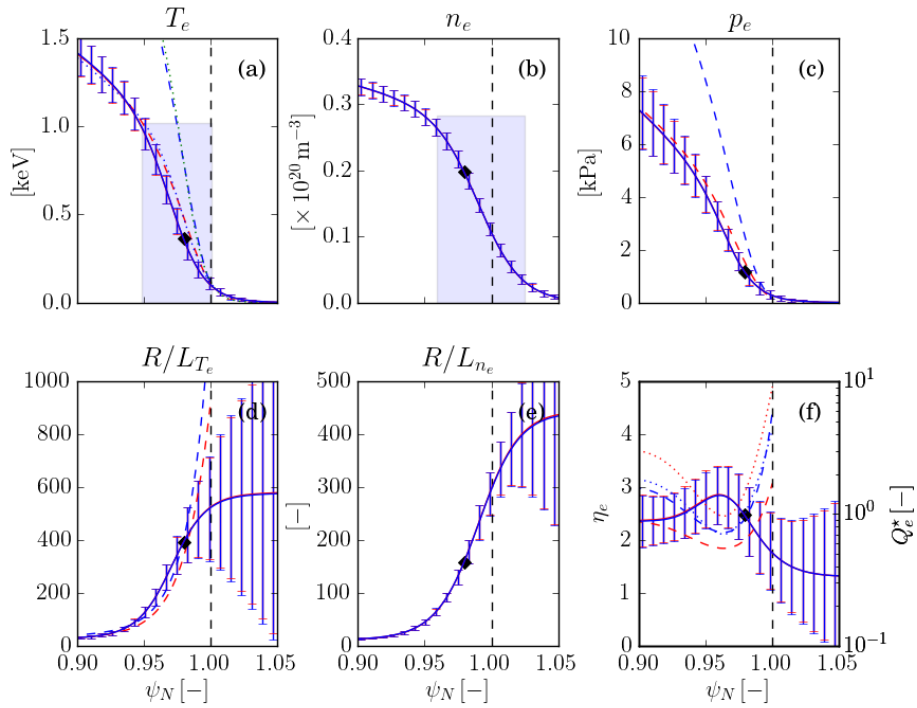


Figure 4. Pre-ELM averaged (80-100% of the inter-ELM period) pedestal profiles for the JET-ILW 3 MA ITER-baseline scenario pulse #94662 with 29 MW of heating power with zero-rate of deuterium gas puffing. Predicted T_e profiles (dashed) calculated using the nominal Q_e^* scaling (cyan) and the stiffer scaling $Q_e^* = 0.85(\eta_e - 0.8)^{2.9}$ (red) are also shown.

the lower current, lower power pulses, with lower gas fuelling rates discussed here, these losses are expected to be still less significant.

Taken together, these observations indicate that: (i) other turbulent modes, e.g. kinetic ballooning modes (KBM) or micro-tearing modes (MTMs), might contribute significantly to the electron heat flux in the region just inside the separatrix; and/or (ii) there may be other relevant parameters governing the scaling of the turbulent electron heat flux due to ETG turbulence, e.g. magnetic shear \hat{s} , which increases strongly close to the separatrix or perhaps the electron collisionality $\nu_{*,e}$.

6. Conclusions

Using the scaling of the locally, gyro-Bohm normalised heat flux Q_e^* with η_e found in Ref. [12] to fit results of non-linear GENE calculations of ETG turbulence for the steep-gradient region of JET-ILW pedestals, it is possible to calculate the T_e profile using the numerical model presented in §3 for the same 1.4 MA pulses for which the scaling was derived with reasonable agreement in terms of the profile shape, pedestal height $T_{e,ped}$ and width Δ_{T_e} .

This model reproduces various observations and dependencies of the pedestal structure: the rather weak dependence of $T_{e,ped}$ on the heating power (at fixed $n_{e,sep}/n_{e,ped}$) and pedestal width Δ_{n_e} ; the different widths $\Delta_{n,T}$ of the T_e and n_e profiles; their relative shift δ_{n-T} ; and how these parameters and $T_{e,ped}$ depend on the relative separatrix density $n_{e,sep}/n_{e,ped}$. However,

there are some obvious discrepancies, i.e. that this scaling over predicts R/L_{T_e} outside the mid-pedestal location and under predicts R/L_{T_e} towards the pedestal top, hence under predicting ΔT_e , although these differences partially compensate yielding a better estimate of $T_{e,ped}$.

Due to the strong dependence of the gyro-Bohm normalisation of the Q_e^* scaling on B^{-2} , $T_{e,ped}$ is predicted to increase with the toroidal field, approximately as $B_t^{2/3}$. Application of the model to a high-power 3.5 MA pulse with twice the toroidal field, significantly underestimated $T_{e,ped}$, which could be resolved either by assuming a lower value of $T_{e,sep}$, which reduces $n_{e,sep}$ or by an up shift of the threshold $\eta_{e,cr}$. An explanation of the sensitivity of $T_{e,ped}$ to the relative separatrix density $n_{e,sep}/n_{e,ped}$ is offered by a simple analytic model of infinitely stiff electron heat transport clamping η_e to the critical threshold across the pedestal.

A further comparison for the case of a wide, low collisionality pedestal of a high-power pulse with zero rate of gas fuelling shows that over prediction of R/L_{T_e} close to the separatrix using the nominal Q_e^* scaling is propagated inwards by the integration, resulting in too high T_e across the pedestal. However, the T_e profile can be well predicted by a modified scaling with $\eta_{e,cr}$ reduced the linear ETG threshold and an increased stiffness exponent. This indicates that the ETG heat flux scaling is not generally valid, so more work on investigating parametric dependence of the normalised electron heat flux Q_e^* on other parameters, e.g. $\hat{s}/q = R/L_s, \dots$ is required.

Such work currently being undertaken by the IFS group [33], attempting to determine a heat flux scaling to fit a database of non-linear GENE turbulence simulations of pedestals from a variety of devices, hints that a stiffer scaling with η_e may be a better fit to the gyro-Bohm normalised heat flux data. Of course, it may well be that other turbulent modes are involved in the electron heat transport, e.g. MTMs at the pedestal top or KBMs at the pedestal foot, so further detailed GK calculations are required to elucidate the underlying heat transport mechanisms.

Work is also underway to incorporate the numerical model of §3 for the T_e profile into EPED. The current implementation assumes a given pedestal density $n_{e,ped}$, decreasing the width Δ_{n_e} until the MHD stability limit is reached, obviating the need to determine the pedestal width using the KBM constraint. This revised model predicts a very strong decrease of the pedestal width Δ_p on the relative separatrix density $n_{e,sep}/n_{e,ped}$, in contrast to the weak dependence predicted by the original EPED model. Further work is underway to compare these differing predictions with measurements. A complete prediction would also require a model for the density profile and for onset of particle and additional heat transport once the total pressure gradient exceeds the KBM stability limit.

Acknowledgements

This work has been carried out within the framework of the EUROfusion Consortium, funded by the European Union via the Euratom Research and Training Programme (Grant Agreement No 101052200 - EUROfusion) and from RCUK Energy Programme [grant No. EP/T012250/1]. Views and opinions expressed are however those of the author(s) only and do not necessarily reflect those of the European Union or the European Commission. Neither the European Union nor the European Commission can be held responsible for them.

References

1. Mailloux J *et al.* 2022 *Overview of JET results for optimising ITER operation*, in press *Nucl. Fusion* ???
2. Wagner F, Becker G, Behringer K, *et al.* 1982 *Phys. Rev. Lett.* **49** 1408
3. Hahm T S and Burrell K H 1995 *Phys. Plasmas* **2** 1648
4. Field A R, Fussmann G, Hofmann J V 1992 *Nucl. Fusion* **32** (7) 1592
5. Field A R *et al.* 2020 *Plas. Phys. Contr. Fusion* **62** 055010
6. Snyder P B, Groebner R J, Leonard A W *et al.* 2009 *Phys. Plasmas* **16** 056118
7. Snyder P B, Wilson H R, Ferron J R *et al.* 2002 *Phys. Plasmas* **9** 2037
8. Connor J W 1985 *Plasma Phys. and Contr. Fusion* **30** 619
9. Jenko F *et al.* 2001 *Phys. Plasmas* **8** 4096

10. Candy J, Belli E A and Bravenec R V 2016 2021 *J. Comput. Phys.* **324** 73
11. Guttenfelder W, Groebner R J, Canik J M *et al.* 2021 *Nucl. Fusion* **61** 056005
12. Chapman B, Hatch D R, Field A R *et al.* *The role of ETG modes in JET-ILW pedestals with varying levels of power and fuelling*, submitted to *Nucl. Fusion* Jan 2022.
13. Romanelli F 1989 *Phys. Fluids B* **1** 1018
14. Luda T *et al.* 2020 *Nucl. Fusion* **60** 036023
15. Schneider P A *et al.* 2013 *Nucl. Fusion* **53** 073039
16. Hatch D R *et al.* 2019 *Nucl. Fusion* **59** 086056
17. Parisi J F *et al.* 2020 *Nucl. Fusion* **60** 126045
18. Görler T, Lapillonne X, Brunner S *et al.* 2011 *Journal of Computational Physics* **230** 7053
19. Barnes M, Parra F I and Schekochihin A A 2011 *Phys. Rev. Lett.* **107** 115003
20. Challis C *et al.* 2015 *Nucl. Fusion* **55** 053031
21. Maggi C F *et al.* 2015 *Nucl. Fusion* **55** 113031
22. Dickinson D *et al.* 2011 *Plasma Phys. and Contr. Fusion* **53** 115010
23. Frassinetti L *et al.* 2012 *Rev. Sci. Inst.* **83** 013506
24. Pasqualotto R *et al.* 2004 *Rev. Sci. Inst.* **75** 10 3891–3893
25. Frassinetti L *et al.* 2018 *Nucl. Fusion* **59** 076038
26. Simpson J *et al.* 2019 *Nucl. Mater. Energy* **20** 100599
27. Appel L C, Lupelli I *et al.* *Comp. Phys. Comm.* **223** 1-17
28. Garzotti L *et al.* 2019 *Nucl. Fusion* **59** 076037
29. Field A R *et al.* 2021 *Plas. Phys. Contr. Fusion* **63** 055013
30. Frassinetti L *et al.* 2021 *Nucl. Fusion* **61** 126054
31. Stefanikova E *et al.* 2018 *Nucl. Fusion* **58** 056010
32. Garcia J *et al.* 2022 *New plasma regimes with small ELMs and high confinement at the Joint European Torus* submitted to *Phys. Plasmas*
33. Hatch D R *et al.* 2021 *Reduced models for ETG transport in the pedestal*, submitted to *Phys. Plasmas* <https://arxiv.org/abs/2201.07831>.